JCI insight

Lymphotoxin β receptor and tertiary lymphoid organs shape acute and chronic allograft rejection

Gang Zhang, … , Khodor I. Abou-Daya, Martin H. Oberbarnscheidt

JCI Insight. 2024. https://doi.org/10.1172/jci.insight.177555.

Research In-Press Preview Immunology Transplantation

Solid organ transplantation remains the life-saving treatment for end-stage organ failure, but chronic rejection remains a major obstacle to long-term allograft outcomes and has not improved substantially. Tertiary lymphoid organs (TLO) are ectopic lymphoid structures that form under conditions of chronic inflammation, and evidence from human transplantation suggests that TLO regularly form in allografts undergoing chronic rejection. In this study, we utilized a mouse renal transplantation model and manipulation of the lymphotoxin alpha (LTα) – lymphotoxin beta receptor (LTβR) pathway, which is essential for TLO formation, to define the role of TLO in transplantation. We showed that intragraft TLO are sufficient to activate the alloimmune response and mediate graft rejection in a model where the only lymphoid organs are TLO in the allograft. When transplanted to recipients with a normal set of secondary lymphoid organs, the presence of graft TLO or LTα overexpression accelerated rejection. If the LTβR pathway was disrupted in the donor graft, TLO formation was abrogated, and graft survival prolonged. Intravital microscopy of renal TLO demonstrated that local T and B cell activation in TLOs is similar to that observed in secondary lymphoid organs. In summary, we demonstrated that immune activation in TLO contributes to local immune responses, leading to earlier allograft failure. TLO and the LTαβ-LTβR pathway are therefore prime targets to limit local immune responses […]

Lymphotoxin beta receptor and tertiary lymphoid organs shape acute and chronic allograft rejection

Gang Zhang[1, 2], Neda Feizi[1], Daqiang Zhao[†], Latha Halesha[1], Amanda L. Williams[1], Parmjeet S. Randhawa[1, 3], Khodor I. Abou-Daya[1], Martin H. Oberbarnscheidt[1, 4‡]

[1]Thomas E. Starzl Transplantation Institute, Department of Surgery, Pittsburgh, PA 15213, USA

[2]Center of Organ Transplantation, Xiangya Hospital, Central South University, Changsha, Hunan 410008, China

[3]Division of Transplant Pathology, Department of Pathology, University of Pittsburgh School of Medicine, Pittsburgh, PA 15213, USA

[4]Department of Immunology, University of Pittsburgh, Pittsburgh, PA 15261, USA

[†]Current address: Tongji Hospital, Tongji Medical College, Huazhong University of Science and Technology, Wuhan, China

[‡]Correspondence:

Martin Oberbarnscheidt, MD PhD

Thomas E. Starzl Transplantation Institute, University of Pittsburgh

200 Lothrop ST

BST W1558

Pittsburgh, PA 15213

United States

Phone: +1-412-648-9547

Email: mho6@pitt.edu

Conflict of Interest: The authors have declared that no conflict of interest exists.

Abstract

Solid organ transplantation remains the life-saving treatment for end-stage organ failure, but chronic rejection remains a major obstacle to long-term allograft outcomes and has not improved substantially. Tertiary lymphoid organs (TLO) are ectopic lymphoid structures that form under conditions of chronic inflammation, and evidence from human transplantation suggests that TLO regularly form in allografts undergoing chronic rejection. In this study, we utilized a mouse renal transplantation model and manipulation of the lymphotoxin alpha (LTα) – lymphotoxin beta receptor (LTβR) pathway, which is essential for TLO formation, to define the role of TLO in transplantation. We showed that intragraft TLO are sufficient to activate the alloimmune response and mediate graft rejection in a model where the only lymphoid organs are TLO in the allograft. When transplanted to recipients with a normal set of secondary lymphoid organs, the presence of graft TLO or LTα overexpression accelerated rejection. If the LTβR pathway was disrupted in the donor graft, TLO formation was abrogated, and graft survival prolonged. Intravital microscopy of renal TLO demonstrated that local T and B cell activation in TLOs is similar to that observed in secondary lymphoid organs. In summary, we demonstrated that immune activation in TLO contributes to local immune responses, leading to earlier allograft failure. TLO and the LTαβ-LTβR pathway are therefore prime targets to limit local immune responses and prevent allograft rejection. These findings are applicable to other diseases such as autoimmunity or tumors, where either limiting or boosting local immune responses is beneficial and improves disease outcomes.

Introduction

In solid organ transplantation, immunosuppressive therapy has substantially improved short-term organ allograft survival by reducing acute rejection rates. However, chronic rejection - mediated by T cells, antibodies (Abs), or both - has not markedly declined in incidence and remains an important obstacle to long-term allograft survival(1, 2). Further understanding of the pathophysiology of chronic rejection is therefore necessary.

A likely important contributor to the pathogenesis of chronic rejection is the formation of tertiary lymphoid organs (TLO) within the graft. TLO are ectopic lymphoid structures resembling lymph nodes (LN) that arise in chronically inflamed tissues by a process called lymphoid neogenesis(3). Pathognomonic features of TLO include distinct T cell zones, B cell zones, and high endothelial venules (HEV), normally not found outside LNs and Peyer's patches. In the non-transplant setting, TLO have been described in autoimmunity, chronic infection, atherosclerosis, and cancer(4). They correlate with disease severity except in cancer, where they portend better prognosis(5, 6). In transplantation, they have been extensively documented in heart, kidney, and lung allografts in both laboratory animals and humans and are associated with chronic rejection and shorter allograft survival(7-10). For example, 78% of mouse heart allografts undergoing chronic rejection, and up to 95% of human renal allograft explants due to chronic rejection have features of lymphoid neogenesis(7, 8). Some reports have also demonstrated roles in tolerance maintenance in mouse models of lung transplantation, where Treg seem to exert their regulatory function in TLO in recipients treated with costimulatory blockade(11). Recent work by Rosales et al. have also described the presence of Treg-rich organized lymphoid structures (TOLS) in a kidney transplantation model in mice using a specific donor – recipient stain combination(12).

These structures, contrary to TLO, do not contain HEVs, reflected by lack of PNAd expression. TOLS have been shown to be important for long-term renal allograft survival, which is dependent on Treg, and can develop in the absence of secondary lymphoid tissue. Although these studies outline specific functions of TLO in different disease models, and associations with specific disease outcomes, cause-effect experiments delineating the contribution of TLO to allograft rejection are sparse.

The lymphotoxin alpha (LTαβ) – lymphotoxin beta receptor (LTβR) pathway is important for lymphoid neogenesis. The ligands for LTβR are the heterotrimer LTα1β2 and LIGHT, while the homotrimer LTα3 can bind to other members of the TNF receptor superfamily (TNFR1, TNFR2 and HVEM). Signaling through LTβR activates the NFκb as well as the JNK pathway. The alternative pathway of NFκb activation involves activation p100, which is dependent on IKKα and NIK and is the major LTβR pathway responsible for lymph node development. This is evident by the absence of secondary lymphoid tissue in LTβR, IKKα and NIK deficient mice. Studies utilizing skin transplantation in recipients that do not have secondary lymphoid organs have demonstrated that skin containing TLO can mediate allograft rejection at the same site or of skin transplanted elsewhere(13).

Despite these different roles of TLO in immunity and allograft rejection, several questions remain: Are TLO contributing to allograft rejection? What immune functions do TLO support in vivo?

In this manuscript, we are utilizing renal allograft transplantation model in mice and manipulation of the LTβR – LTαβ pathway to elucidate the role of TLO in allograft rejection. Moreover, we developed an intravital microscopy model to visualize immune cell interactions in renal TLO to investigate if TLO support activation of T and B cells. We found that TLO are

sufficient for renal allograft rejection, that they contribute to rejection even in the presence of lymph nodes and that disrupting the LTβR pathway prolongs allograft survival. Intravital microscopy showed that TLO support T and B cell activation.

Results

TLO are sufficient for renal allograft rejection

To investigate if renal TLO are sufficient to initiate an alloimmune response and cause graft rejection, we utilized splenectomized LTβR-deficient (LTβR-ko) mice as recipients of F1 (B6 x Balb/c, CB6F1) or F1-RIP-LTα kidneys (Figure 1A). LTβR-ko mice do not have lymph nodes or peyer's patches and after splenectomy are devoid of all secondary lymphoid organs. Secondary lymphoid organs are necessary to mount an alloimmune response and reject an allograft(14). F1-RIP-LTα mice express lymphotoxin alpha under control of the rat insulin promoter and develop spontaneous TLO in the pancreas, skin, and kidney at 4 to 6 months of age(15). F1-RIP-LTα donor kidneys therefore contain preformed TLO at the time of transplantation, while F1 WT kidneys do not. In this model, the only lymphoid tissue present is the TLO in the donor graft. To rule out that the presence of inflammatory TLO or LTα overexpression in the donor graft has a functional consequence independent of an alloimmune response, we performed syngeneic F1-RIP-LTα kidney transplants to F1 recipients as controls. As shown in Figure 1B, F1 allografts survive beyond 200 days, while F1-RIP-LTα grafts containing TLOs are rejected with a mean survival time (MST) of 23 days. Syngeneic F1-RIP-LTα grafts were maintained beyond day 90. Donor specific antibody measurements in the serum on day 50 show lack of DSA in recipients of WT allografts while IgG DSA was present in recipients that received F1-RIP-LTα allografts, suggesting that TLO provide a place for B cell activation and antibody formation (Figure 1C). Histopathology (Figure 1D) demonstrates the presence of TLO pre-transplantation as well as at time of rejection in F1 RIPLTα allografts. F1 allografts show less infiltration and lower proportions of severe rejection (Banff >1B) (Figure 1, E and F) on day 200 but are characterized by the presence of lymphoid aggregates around small

arteries. Syngeneic F1-RIP-LTα grafts display presence of TLO before and after transplantation, but no other immune infiltrate (Figure 1D) and surpass rejection time of the F1-RIPLTα allografts transplanted to LTβR$^{-/-}$ recipients. Treg-rich organized lymphoid structures (TOLS) have been previously documented, notably even in the absence of secondary lymphoid tissue(12). To further characterize the lymphoid aggregates present in allografts, we performed IF staining for T, B, FoxP3 and PNAd in both F1 and F1-RIP-LTα grafts. As shown in Supplemental Figure 1, lymphoid aggregates in F1 allografts are characterized by T and B cell areas, the presence of FoxP3^{+} Treg and the absence of PNAd, fulfilling the main criteria for TOLS. Lymphoid aggregates in F1-RIPLTα grafts also contain T and B cell areas, but lack FoxP3^{+} Treg cells. In addition, PNAd staining is present in these structures, a hallmark of inflammatory tertiary lymphoid organs. The long-term life sustaining function of the syngeneic F1-RIP-LTα kidney grafts suggests that graft failure in allogeneic kidney transplants is a consequence of rejection rather than the mere presence of TLO or LTα overexpression in the graft. These data demonstrate that preformed TLO are sufficient for allograft rejection and support a full alloimmune response with T and B cell activation / DSA production.

TLO accelerate renal allograft rejection

We next investigated if TLO contribute to renal allograft rejection in the presence of a normal set of secondary lymphoid tissue. We transplanted either F1 or F1-RIPLTα kidneys to WT B6 recipients and monitored allograft survival (Figure 2A). As LTα can bind as a heterotrimer LTα1β2 to LTβR and as a homotrimer LTα3 to TNFR family members, mediating inflammatory signals, we also transplanted F1-RIPLTα kidneys from young donors (8 weeks old), in which no TLO have formed at the time of transplantation, but LTα is overexpressed. Allograft survival of

F1-RIPLTα kidneys was significantly shorter (MST=63 days) than survival of F1 allografts (MST=225 days), indicating that preformed TLO in the graft accelerate allograft rejection (Figure 2B). Renal allografts from young F1-RIPLTα donors were also rejected significantly earlier (MST=72.5 days) than F1 allografts. No significant differences were detected in DSA formation (Figure 2C). Histopathology at the time of rejection demonstrated the presence of TLO in all allografts. F1-RIPLTα grafts displayed prominent TLO pre- and post-transplantation. In young F1-RIPLTα donor grafts, only occasional lymphoid aggregates were present pre-transplantation, but TLO developed quickly post-transplantation (Figure 2D), which makes it impossible to separate the inflammatory effects of LTα from TLO functions. F1 allografts demonstrated development of TLO with HEV (PNAd expression) (Supplemental Figure 2) at the time of rejection, suggesting that de novo TLO formation in WT grafts requires a longer time to occur (Figure 2D). Histological quantitation of the cellular infiltrate (Figure 2E) and Banff rejection scores (Figure 2F) confirmed that the presence of preformed or rapidly forming TLO in the allograft leads to a larger immune infiltrate and higher Banff scores, reflecting the differences in median survival time. These data support that TLO and LTα-LTβR signaling contribute to chronic allograft rejection in WT recipients.

Blocking donor LTβR signaling prolongs allograft survival

To further elucidate the role of TLO in allograft rejection, we performed transplantation survival experiments where donor LTβR signaling is disrupted. LTβR is critically important for secondary lymphoid organ and TLO formation and binds two different ligands, the heterotrimeric LTα1β2 and LIGHT. While the heterotrimer LTα1β2 only binds to LTβR, the LTα3 homotrimer has inflammatory properties similar to TNFα, binds to TNFRI, II and HVEM,

but not to LTβR. LTα3 has been associated with autoimmunity and inflammatory diseases. In this model, we are therefore able to separate the proinflammatory effects of LTα3 signaling from the effects of blocking LTβR signaling. We used B6 WT or B6 LTβR-ko donor grafts transplanted to Balb/c recipients (Figure 3A). The B6 to Balb/c kidney transplantation model results in acute rejection of renal allografts. As LTβR expression on stromal cells is essential for lymphoid neogenesis, the absence of LTβR on donor graft tissue prevents intragraft TLO formation and inflammatory signals mediated through LTβR. As shown in Figure 3B, B6 WT allografts are quickly rejected (MST=11 days), while B6 LTβR-ko allografts survive significantly longer (MST=24 days). No statistically significant difference in IgG DSA production in the B6 WT allograft recipients compared to B6 LTβR-ko graft recipients were observed (Figure 3C). Histopathology of a subset of grafts procured on day 9 after transplantation showed more severe immune cell infiltration in B6 WT allografts compared to B6 LTβR-ko allografts (Figure 3D). Immunofluorescence for PNAd showed presence of HEV in B6 allografts but not in B6 LTβR-ko allografts, indicating that B6 WT renal allografts promote lymphoid neogenesis very early after transplantation (Figure 3D). Quantitation of the immune infiltrate at the time of rejection revealed a significant higher infiltration in B6 WT compared to B6 LTβRko allografts (Figure 3E), and Banff rejection scores at the time of rejection were significantly higher (>IB compared to <IA)) in B6 than in B6 LTβR-ko allografts (Figure 3F).

Renal TLO support naïve immune cell activation

To further investigate the function of TLO, we developed an intravital microscopy model to study cell-cell interactions in vivo in TLO under the kidney capsule. This allowed us to compare immune cell interactions in TLO to that observed in lymph nodes. We imaged kidneys of bone

marrow chimeric CD11c-YFP B6 RIP-LTα mice, where we could identify TLO by (a) the lack of normal kidney structure (capillaries), and (b) the accumulation of CD11c-YFP+ dendritic cells. To clearly define the time point of antigen introduction, we utilized transgenic OT-I (dsRed) and OT-II (CFP) T and NP-specific (CellTracker Red) B cells, imaged at time 0, and after 1, 3, 6, 24 and 72 hours after immunization with either anti-DEC-205 (OT-I T cells) or NP-Ovalbumin (OT-II and B cells) (Figure 4A). As shown in Figure 4B, TLO can be identified by MAdCAM-1 expression (HEV), accumulation of dendritic cells, presence of naïve T or B cells, which are absent in normal surrounding kidney tissue, and lack of normal kidney tissue structure. Naïve T and B cells accumulate in distinct zones (Figure 4B). We first evaluated motility parameters of OT-I T cells before and after immunization with anti-DEC205-OVA and FGK4.5(16). OT-I T cells displayed a reduction in mean speed and displacement after immunization and an increased arrest coefficient over time (Figure 4C and Supplemental Movie 1), which is reflected in total track length shown in the bottom panel of Figure 4C. To investigate B cell activation, we transferred NP-specific B cells (labeled with CellTracker Red) and OT-II T cells (CFP) and performed imaging at day 0, and days 1 and day 3 after immunization with NP-ovalbumin and adjuvant. For B cells, we observed an increase in motility and displacement after immunization, which is similar to observations made in lymph nodes and consistent with B cell activation (Figure 4D and Supplemental Movie 2)(17, 18). CD4 OT-II T cells were imaged at the same time points and displayed lower mean speed and increased arrest coefficient on day 1 after immunization with increased motility parameters on day 3 (Figure 4E and Supplemental Movie 3) and associated changes in total track length (Figure 4E, bottom row). The observations in T cells are indicative of stable cell-cell interactions needed for activation and similar to motility changes that have been observed during T cell activation in lymph nodes (19, 20).

Discussion

The formation of TLO through the process of lymphoid neogenesis has long been associated with chronic inflammatory conditions where antigen persists(21). This is the case during chronic infections, autoimmune diseases, and organ transplantation(22-25). The discovery that many cancers also promote TLO formation and that the presence of TLO often is a predictor of better outcomes, has led to a resurgence of interest in TLO(26). TLO have immunomodulatory effects, they can either promote immunity or can be associated with immune regulation(11, 27, 28). In transplantation, TLO have been associated with both, chronic rejection outcomes and graft acceptance, at least in animal models(7, 11, 13, 27). In this study, we have performed cause-effect experiments to further define the role of TLO in acute and chronic rejection in a mouse model of kidney transplantation. We are not only defining the role of TLO by manipulating the LTα – LTβR pathway in survival experiments, but also developed a model of intravital microcopy to capture for the first time the cellular events and interactions in TLO, similar to what has been studied in lymph nodes.

We demonstrate that TLO are sufficient to mediate allograft rejection in recipients that do not have secondary lymphoid tissue and do not reject allografts in the absence of TLO. This highlights that TLO are fully functional lymphoid organs that are capable of providing the environment needed for activation of an adaptive immune response in a model of vascularized, solid organ transplantation. This includes the activation of B cells and production of donor-specific antibodies (DSA), which do not develop if WT, non-TLO containing, allografts are transplanted. The chronic kidney transplantation model used in our studies is not dependent on DSA, of which we are only able to detect low levels in the serum, independent of the presence of

preformed graft TLO. The significance of B cell activation and DSA production in graft TLO needs to be further investigated.

We observed that F1 allografts, although maintained long-term and not undergoing rejection, contained lymphoid aggregates that resemble the Treg-rich organized lymphoid structures (TOLS) that have been previously reported(12). Our data confirm that TOLS can form in a donor - recipient strain combination where the recipient lacks secondary lymphoid tissue as first described by Rosales et al (12). These aggregates were characterized by the presence of Treg, the absence of HEV expressing PNAd and a location around a central blood vessel. These aggregates were not present when F1 allografts were transplanted to B6 WT recipients, where we observed formation of inflammatory TLO over time. The formation of TOLS in renal allografts transplanted to LTβR$^{-/-}$ recipients offers an opportunity for further research to elucidate what conditions and mechanisms govern their formation and function.

This study demonstrates that TLO accelerate allograft rejection in the presence of a normal set of secondary lymphoid tissue. While WT F1 allografts also demonstrated TLO at the time of rejection, there was a marked difference in rejection tempo if TLO were present at the time of transplantation, suggesting a local contribution of TLO in the alloimmune response. A caveat of TLO studies is that the function of TLO is linked to local inflammation, as a chronic inflammatory environment is essential to provide the conditions necessary for the development of TLO. This is also applicable to the model utilized in this study. The RIP-LTα model causes local overexpression of the inflammatory mediator LTα, which then provides the signal for TLO formation. We attempted to address this by transplanting donor kidneys from young F1 RIP-LTα

mice which did not harbor TLO at the time of transplantation, but the histological presence of TLO after accelerated allograft rejection confirmed that the function of TLO and inflammatory signals could not be separated in this experiment. A separate TLO-independent function of LTα can therefore not be ruled out.

In an acute kidney rejection model (B6 to Balb/c), disrupting the LTβR pathway in donor allografts led to prolonged allograft survival compared to WT B6 donors. Prolongation of allograft survival took place with intact LTα3 and TNFα signaling pathways that mediate inflammatory signals, which highlights the importance of the LTβR pathway in allograft rejection. The outcome of prolonged allograft survival cannot be attributed solely to lymphoid neogenesis as LTβR signaling involves activation of both, the NFκB and JNK pathways, which play roles not only in lymphoid neogenesis but also mediate inflammatory signals. It is therefore possible that not only the prevention of TLO formation is causative for better allograft survival, but that the absence of inflammatory signals mediated though LTβR also contribute to this outcome. However, physiologically the presence of TLO is intrinsically linked to inflammatory signals, making TLO and the LTβR pathway relevant targets to improve allograft outcomes.

The intravital microscopy data of TLO in this model suggests that productive cell-cell interactions, leading to activation of naïve T cells, are taking place in TLO. Together with the survival data presented, TLO are therefore likely to contribute to local immune activation and maintenance in this model. As the cell-cell interactions and motility parameters observed in TLO are similar to what has been described in lymph nodes, it is likely that TLO support similar immunological functions, including promoting regulatory functions under the appropriate

conditions. It is promising that interfering with the LTβR pathway in the donor organ can delay allograft rejection significantly in an acute kidney graft rejection model in mice. This work used transplantation as a model to investigate the function of TLO, but the results are equally relevant to autoimmunity, cancer, and other chronic inflammatory conditions.

Methods

Sex as a biological variable

Both sexes of mice were used, but males were preferred for the transplantation procedure due to size and anatomy. Previous studies have not identified sex differences in allograft rejection beyond the known H-Y minor histocompatibility Ag in the absence of an MHC mismatch. The findings obtained in this study are expected to be relevant to both sexes.

Study design

Three biological replicates (3 individual transplant recipients) per group were included in each experiment. Experiments were repeated once resulting in a total of up to 6 biological replicates. Sample sizes were based on prior observations that three to six biological replicates were sufficient to discern statistically significant differences between groups, with observed effect sizes >0.5. Prospective exclusion criteria were transplant recipient death within the first 7 days after transplantation (technical failure) and urinary obstruction (censored data points). All other data points were included, and no outliers were excluded. All end points were prospectively selected. It was not possible to blind the study because of the need to identify donors and recipients. Histopathological scoring was blinded.

Animals

B6.CD45.2 (C57BL/6J; Thy1.2, CD45.2), B6.CD45.1 (B6.SJL-*Ptprc*^{a}*Pepc*^{b}/BoyJ, Thy1.2, CD45.1), DsRed [B6.Cg-Tg(CAG-DsRed*MST)1Nagy/J], Balb/c CD45.1 (CByJ.SJL(B6)-Ptprca/J), F1 (CB6F1/J), B6 CD11c-YFP (B6.Cg-Tg(Itgax-Venus)1Mnz/J) were from Jackson Laboratory (Jax). B6.CD45.1 (B6.SJL-*Ptprc*^{a}*Pepc*^{b}/BoyCrl) were from Charles River Laboratories. B6 RIP-LTα mice were maintained and bred at the University of Pittsburgh and

were originally from Nancy Ruddle (Yale University). B6 B18 NP-specific B cell transgenic mice were from Mark Shlomchik (Department of Immunology, University of Pittsburgh, Pittsburgh). B6 OT-II (B6.Cg-Tg(TcraTcrb)425Cbn/J) mice (Jackson Laboratories) were crossed to B6.CFP (B6.129(ICR)-Tg(CAG-ECFP)CK6Nagy/J) and maintained on a B6 Rag-deficient background. B6 OT-I mice (C57BL/6-Tg[TcraTcrb]1100Mjb/J; CD45.2) were obtained from Jax and maintained on a RAG$^{-/-}$ DsRed background. B6 LTβR$^{-/-}$ were maintained and bread at the University of Pittsburgh and were originally received from the University of Chicago. Transplant recipients were 8-12 weeks old, RIP-LTα mice were used at age 5-8 months when TLO were consistently present. Some experiments utilized young RIP-LTα mice (8 weeks).

Kidney transplantation and nephrectomy

Mouse kidney transplants were performed as previously described (29). Recipient native kidneys were removed during the transplantation procedure. Allograft rejection was monitored by visual observation of recipients for signs of uremia (lethargy, decreased mobility, and ruffled hair) or death.

Bone marrow chimeras

CD11c-YFP bone marrow chimeras were generated by irradiating B6.RIP-LTα mice with 10 Gy followed by adoptive transfer 10×10^6 BM cells i.v. from CD11c-YFP. Mice received sulfatrim food for 14 days after irradiation. Reconstitution was confirmed 56 days after bone marrow transplantation by visualizing tissue turn-over of tissue dendritic cells using YFP fluorescence.

Histological analysis and Immunofluorescence staining

Kidney allograft tissue was fixed in formalin, paraffin-embedded, sectioned, and stained with hematoxylin and eosin (H&E), Masson's trichrome (MT), and periodic acid–Schiff (PAS) stain (Magee-Women's Research Institute Histology and Microimaging Core, University of Pittsburgh). For Immunofluorescence, cryosections were stained with primary antibodies for 16 hours at 4°C. Following avidin/biotin blocking, slides were incubated with biotinylated secondary antibody for 30 minutes at room temperature, and then streptavidin-conjugated quantum dots for 30 minutes at room temperature. For FFPE tissue, sections were deparaffinized, and antigen retrieval was performed at pH 6 for 30 min at 96ºC (Target Retrieval Solution pH6, Agilent) followed by blocking with FBS and 5% rat serum. Sections were then stained with primary antibodies (PNAd (biotin, clone MECA-79, BioLegend), CD3 (rabbit, cat#A0452, Agilent) and B220 (AF488, clone RA3-6B2, eBioscience) and secondary antibodies (streptavidin-AF647, goat anti-rabbit IgG H+L (Invitrogen, cat# A-11012, AF594). FoxP3 staining was performed after additional 1% Triton X-100 incubation for 30 min, followed by FoxP3-AF647 (BioLegend, clone 150D). DAPI was used to visualize nuclei. Stained sections were mounted in EcoMount (Biocare Medical). All slides were scanned on a Zeiss Axioscan.Z1 with a 20× objective and analyzed in QuPath (30). A pixel classifier was trained in QuPath to quantitate immune infiltration per kidney section at time of rejection, using H&E-stained sections. Histological sections of allografts were scored according to Banff classification.

Donor-reactive antibody detection

Donor-specific antibodies were detected by incubating recipient serum with donor splenocytes and detecting bound antibodies with ani-mouse IgG-FITC antibody (Life Technologies, cat# 11-4011-85). Briefly, donor F1 splenocytes were incubated with 20% FBS for 20 min at RT to block

non-specific binding. Recipient serum (25 µl) was added to 0.5 x 10^6 donor splenocytes and incubated on ice for 1 hour. Cells were washed and surface staining for CD3-PE (eBioscience, clone 145-2C11), B220-eF450 (eBioscience, clone RA3-6B2) and anti-IgG performed. Samples were acquired on a BD Fortessa or Cytek Aurora spectral cytometer. Alloantibody binding was assessed on T cells and MFI reported (Supplemental Figure 3).

Two-Photon Intra-Vital Imaging

Multi-photon intravital microscopy was performed on transplanted kidneys. A custom Leica TCS SP8 Triple Beam 6 Ch NDD system containing 6 HyD detectors, and two Spectra Physics femto-second pulsed lasers (MaiTai DeepSee and Insight X3) with three laser lines was used. Laser was tuned and mode-locked to 920 nm. The following filter sets were used: 583/22 (dsRed), 537/26 (EYFP), 483/32 (CFP) and 655/15 (Evans Blue). Microscope data was acquired with Leica LAS X v2.53. Mice were anesthetized with isoflurane and oxygen and core body temperature maintained at 37ºC with a homeothermic controller (TC-1000, CWE, Ardmore, PA). Animals were kept hydrated by injecting 1 ml 5% dextrose lactated ringer's solution s.c. every 60 min. Blood vessels were visualized by injecting Evans Blue (3-6 µl of 5 mg/ml stock solution (15-30 µg) diluted in PBS i.v.), HEV were visualized by injecting 3 µg of PE-conjugated MAdCAM-1 antibody i.v. (Biolegend, clone MECA367). The kidney was extraverted from the abdominal cavity with intact vascular connection and immobilized in a custom cup mount. A coverslip was placed on top of the kidney and z-stacks were visualized with a 25x water immersion objective (NA: 1.05) up to 70 µm below the kidney capsule. All stacks were acquired with a step size of 1 µm. Brightness and laser power were adjusted based on the imaging depth and kept below phototoxic levels. Line averaging was set to 4x at a resolution of 512x512 pixel using the

resonance scanner. Time-lapse imaging was performed for ~30 min per location. Up to five different locations per kidney graft were imaged. All acquired movies were analyzed using Imaris software V9 (Oxford Instruments). Drift was corrected using dendritic cells or vasculature as a reference point. Background subtraction was performed on all channels equally.

Statistics and reproducibility

Statistical analysis was performed using Prism v.9 (GraphPad). Parametric and non-parametric tests were used as indicated in figure legends. Categorical data was analyzed using Fisher's exact test where indicated. All *p* values, regardless of statistical significance, were reported.

Study approval

All animal experiments were performed with approval and under supervision of the Institutional Animal Care and Use Committee of the University of Pittsburgh, protocol# 20107883, Animal Welfare Assurance, number D16-00118 (A3187-01).

Data availability

All data point values are available in the Supporting Data Values file.

Author Contributions

MHO conceived studies and designed experiments. GZ, NF, DZ and KIA conducted experiments. GZ and DZ performed mouse kidney transplant procedures. MHO, NF, and KIA analyzed and interpreted data. LH performed immunofluorescence staining, LH and ALW performed flow cytometry and genetic typing of mice. PR conducted the histological analysis and scoring. MHO wrote the manuscript. All authors contributed to reviewing and editing the manuscript.

Acknowledgements

This work was supported by NIH grant AI145881 to MHO. KIA was supported by the 2020 Stuart K. Patrick Grant for Transplant Innovation and the 2023 American Society of Transplantation Career Transition Grant (Grant #998676). NF was supported by the American Society of Transplantation Sanofi Basic Science Fellowship Research Grant. The Unified Flow Core at the University of Pittsburgh is supported by NIH grants S10OD032265 and S10OD030396.

Figure legends:

Figure 1: TLO are sufficient for renal allograft rejection.

(A) F1 (n=7) or F1.RIP-LTα (n=6) donor kidneys were transplanted to splenectomized B6 LTβR-ko mice and graft survival monitored. **(B)** Kaplan-Meier curve of graft survival. Median survival time (MST) of F1.RIP-LTα grafts = 23 days. Recipients of F1 allografts were sacrificed on day 200 with functioning graft. F1 recipients of syngeneic F1-RIPLTα grafts were sacrificed on day 90 with functioning grafts. Sample size n=6-7. $P<0.0001$, determined by log-rank (Mantel-Cox) test. **(C)** Flow cytometric assay assessing serum IgG DSA of graft recipients. P values were determined by one-way ANOVA with multiple comparisons. **(D)** Representative images of H&E-stained sections of allograft tissue at indicated time points after transplantation. Pre-transplant native kidney images from the same donor strain shown for reference. Scale bars = 500 μm. **(E)** Histological quantitation of immune infiltration. P values were determined by one-way ANOVA with multiple comparisons. **(F)** Banff rejection scores of histology procured at time of graft failure. P values were determined by Fisher's exact test.

Figure 2: Preformed TLO accelerate renal allograft rejection

(A) F1 or F1.RIPLTα donor kidneys were transplanted to B6 recipients. Young F1.RIPLTα donors were 8 weeks old and kidneys did not contain TLO at the time of transplantation. **(B)** Kaplan-Meier curve of graft survival. F1 MST=225 days (n=8), F1.RIPLTα MST=63 days (n=6), young F1.RIPLTα MST=72.5 days (n=4). Syngeneic B6 grafts shown as controls (MST>200 days, n=9). P values determined by log-rank (Mantel-Cox) test. **(C)** Flow cytometric assay assessing serum IgG DSA of graft recipients 60 days after transplantation. P values were determined by one-way ANOVA with multiple comparisons. **(D)** Representative images of

H&E-stained sections of allograft tissue at indicated time points after transplantation. Pre-transplant native kidney images from the same donor strain shown for reference. Scale bars = 500 μm. **(E)** Histological quantitation of immune infiltration. P values were determined by one-way ANOVA with multiple comparisons. **(F)** Banff rejection scores of histology procured at time of graft failure. P values were determined by Fisher's exact test.

Figure 3: Blocking donor LTβR signaling prolongs allograft survival

(A) B6 or B6.LTβR-ko donor kidneys were transplanted to Balb/c recipients. **(B)** Kaplan-Meier curve of graft survival. B6 MST=11 days (n=7), B6.LTβR-ko MST=24 days (n=7). P values determined by log-rank (Mantel-Cox) test. **(C)** Flow cytometric assay assessing serum IgG DSA of graft recipients 9 days after transplantation. P values were determined by one-way ANOVA with multiple comparisons. **(D)** Top row: Representative images of H&E-stained sections of allograft tissue at indicated time points after transplantation. Bottom row: Representative immunofluorescence images with PNAd (magenta) and DAPI (blue) staining of allograft tissue on day 9 after Tx. LN shown as control. Scale bars = 100 μm. **(E)** Left: Histological quantitation of immune infiltration. P values were determined by one-way ANOVA with multiple comparisons. Right: Banff rejection scores of histology procured at time of graft failure. P values were determined by Fisher's exact test.

Figure 4: Intravital microscopy of TLO and immune cell interactions

(A) Experimental design of imaging experiments: 10 million OT-I dsRed CD8 T cells or 10 m OT-II CFP CD4 T cells and 30 m NP-specific B1.8 B cells labeled with CellTracker FarRed were adoptively transferred to naïve B6.RIPLTα mice one day before imaging. TLO were

imaged at time 0 (before antigen administration) and at indicated times after immunization. Sample size n=3 animals per time point, n=3-6 time lapse recordings per animal. **(B)** Intravital microscopy images depicting (A) MAdCAM-1 staining limited to a TLO (dotted line) with surrounding normal kidney tissue. Capillaries (cyan), dendritic cells (green). (B) TLO with dendritic cells (green) and OT-I CD8 T cells (red). Collagen fibers (blue, second harmonic signal). (C) TLO with OT-II CD4 T cells (blue), B cells (red) and dendritic cells (green). Collagen (blue). **(C)** CD8 T cell motility parameters. Top: quantitation of mean speed, displacement, and arrest coefficient of CD8 OT-I T cells at indicated time points. Bottom: Representative images depicting tracks of OT-I CD8 T cells at different time points. P values were determined using one-way ANOVA with Tukey's multiple comparison test. **(D)** Analysis of B cell motility parameters. Top: Quantitation of mean speed, displacement, and arrest coefficient of B1.8 B cells at indicated time points after antigen administration. Bottom: Representative images with total B cell track lengths depicted in white at indicated time points. **(E)** Analysis of OT-II motility parameters. Top: Quantitation of mean speed, displacement, and arrest coefficient of OT-II CD4 T cells at indicated time points. Bottom: Representative images depicting total CD4 T cell track lengths in white at indicated time points. P values were determined using one-way ANOVA with Tukey's multiple comparison test.

References

1. Hart A, Smith JM, Skeans MA, Gustafson SK, Wilk AR, Robinson A, et al. OPTN/SRTR 2016 Annual Data Report: Kidney. *Am J Transplant.* 2018;18 Suppl 1:18-113.
2. Hariharan S, Israni AK, and Danovitch G. Long-Term Survival after Kidney Transplantation. *N Engl J Med.* 2021;385(8):729-43.
3. Ruddle NH. Lymphoid neo-organogenesis: lymphotoxin's role in inflammation and development. *Immunol Res.* 1999;19(2-3):119-25.
4. Drayton DL, Liao S, Mounzer RH, and Ruddle NH. Lymphoid organ development: from ontogeny to neogenesis. *Nat Immunol.* 2006;7(4):344-53.
5. Lin L, Hu X, Zhang H, and Hu H. Tertiary Lymphoid Organs in Cancer Immunology: Mechanisms and the New Strategy for Immunotherapy. *Front Immunol.* 2019;10:1398.
6. Hiraoka N, Ino Y, Yamazaki-Itoh R, Kanai Y, Kosuge T, and Shimada K. Intratumoral tertiary lymphoid organ is a favourable prognosticator in patients with pancreatic cancer. *Br J Cancer.* 2015;112(11):1782-90.
7. Baddoura F, Nasr I, Wrobel B, Li Q, Ruddle N, and Lakkis F. Lymphoid neogenesis in murine cardiac allografts undergoing chronic rejection. *Am J Transplantation.* 2005;5:510-6.
8. Thaunat O, Patey N, Caligiuri G, Gautreau C, Mamani-Matsuda M, Mekki Y, et al. Chronic rejection triggers the development of an aggressive intragraft immune response through recapitulation of lymphoid organogenesis. *J Immunol.* 2010;185(1):717-28.
9. Thaunat O, Field A-C, Dai J, Louedec L, Patey N, Bloch M-F, et al. Lymphoid neogenesis in chronic rejection: Evidence for a local humoral alloimmune response. *Proc Natl Acad Sci U S A.* 2005;102:14723-8.
10. Sato M, Hirayama S, Hwang DM, Lara-Guerra H, Wagnetz D, Waddell TK, et al. The role of intrapulmonary de novo lymphoid tissue in obliterative bronchiolitis after lung transplantation. *J Immunol.* 2009;182(11):7307-16.
11. Li W, Bribriesco AC, Nava RG, Brescia AA, Ibricevic A, Spahn JH, et al. Lung transplant acceptance is facilitated by early events in the graft and is associated with lymphoid neogenesis. *Mucosal Immunol.* 2012;5(5):544-54.
12. Rosales IA, Yang C, Farkash EA, Ashry T, Ge J, Aljabban I, et al. Novel intragraft regulatory lymphoid structures in kidney allograft tolerance. *Am J Transplant.* 2022;22(3):705-16.
13. Nasr IW, Reel M, Oberbarnscheidt MH, Mounzer RH, Baddoura FK, Ruddle NH, and Lakkis FG. Tertiary lymphoid tissues generate effector and memory T cells that lead to allograft rejection. *Am J Transplant.* 2007;7(5):1071-9.
14. Lakkis FG, Arakelov A, Konieczny BT, and Inoue Y. Immunologic 'ignorance' of vascularized organ transplants in the absence of secondary lymphoid tissue. *Nat Med.* 2000;6(6):686-8.
15. Kratz A, Campos-Neto A, Hanson MS, and Ruddle NH. Chronic inflammation caused by lymphotoxin is lymphoid neogenesis. *J Exp Med.* 1996;183(4):1461-72.
16. Bonifaz L, Bonnyay D, Mahnke K, Rivera M, Nussenzweig MC, and Steinman RM. Efficient targeting of protein antigen to the dendritic cell receptor DEC-205 in the steady state leads to antigen presentation on major histocompatibility complex class I products and peripheral CD8+ T cell tolerance. *J Exp Med.* 2002;196(12):1627-38.
17. Qi H, Egen JG, Huang AY, and Germain RN. Extrafollicular activation of lymph node B cells by antigen-bearing dendritic cells. *Science.* 2006;312(5780):1672-6.
18. Okada T, Miller MJ, Parker I, Krummel MF, Neighbors M, Hartley SB, et al. Antigen-engaged B cells undergo chemotaxis toward the T zone and form motile conjugates with helper T cells. *PLoS Biol.* 2005;3(6):e150.

19. Stoll S, Delon J, Brotz TM, and Germain RN. Dynamic imaging of T cell-dendritic cell interactions in lymph nodes. *Science.* 2002;296(5574):1873-6.
20. Shakhar G, Lindquist RL, Skokos D, Dudziak D, Huang JH, Nussenzweig MC, and Dustin ML. Stable T cell-dendritic cell interactions precede the development of both tolerance and immunity in vivo. *Nat Immunol.* 2005;6(7):707-14.
21. Aloisi F, and Pujol-Borrell R. Lymphoid neogenesis in chronic inflammatory diseases. *Nat Rev Immunol.* 2006;6(3):205-17.
22. Bombardieri M, Lewis M, and Pitzalis C. Ectopic lymphoid neogenesis in rheumatic autoimmune diseases. *Nat Rev Rheumatol.* 2017;13(3):141-54.
23. Koenig A, and Thaunat O. Lymphoid Neogenesis and Tertiary Lymphoid Organs in Transplanted Organs. *Front Immunol.* 2016;7:646.
24. Pitzalis C, Jones GW, Bombardieri M, and Jones SA. Ectopic lymphoid-like structures in infection, cancer and autoimmunity. *Nat Rev Immunol.* 2014;14(7):447-62.
25. Ruddle NH. Posttransplant Tertiary Lymphoid Organs. *Transplantation.* 2023.
26. Schumacher TN, and Thommen DS. Tertiary lymphoid structures in cancer. *Science.* 2022;375(6576):eabf9419.
27. Brown K, Sacks SH, and Wong W. Tertiary lymphoid organs in renal allografts can be associated with donor-specific tolerance rather than rejection. *Eur J Immunol.* 2011;41(1):89-96.
28. Kang W, Feng Z, Luo J, He Z, Liu J, Wu J, and Rong P. Tertiary Lymphoid Structures in Cancer: The Double-Edged Sword Role in Antitumor Immunity and Potential Therapeutic Induction Strategies. *Front Immunol.* 2021;12:689270.
29. Abou-Daya KI, Tieu R, Zhao D, Rammal R, Sacirbegovic F, Williams AL, et al. Resident memory T cells form during persistent antigen exposure leading to allograft rejection. *Science immunology.* 2021;6(57).
30. Bankhead P, Loughrey MB, Fernández JA, Dombrowski Y, McArt DG, Dunne PD, et al. QuPath: Open source software for digital pathology image analysis. *Scientific reports.* 2017;7(1):16878.

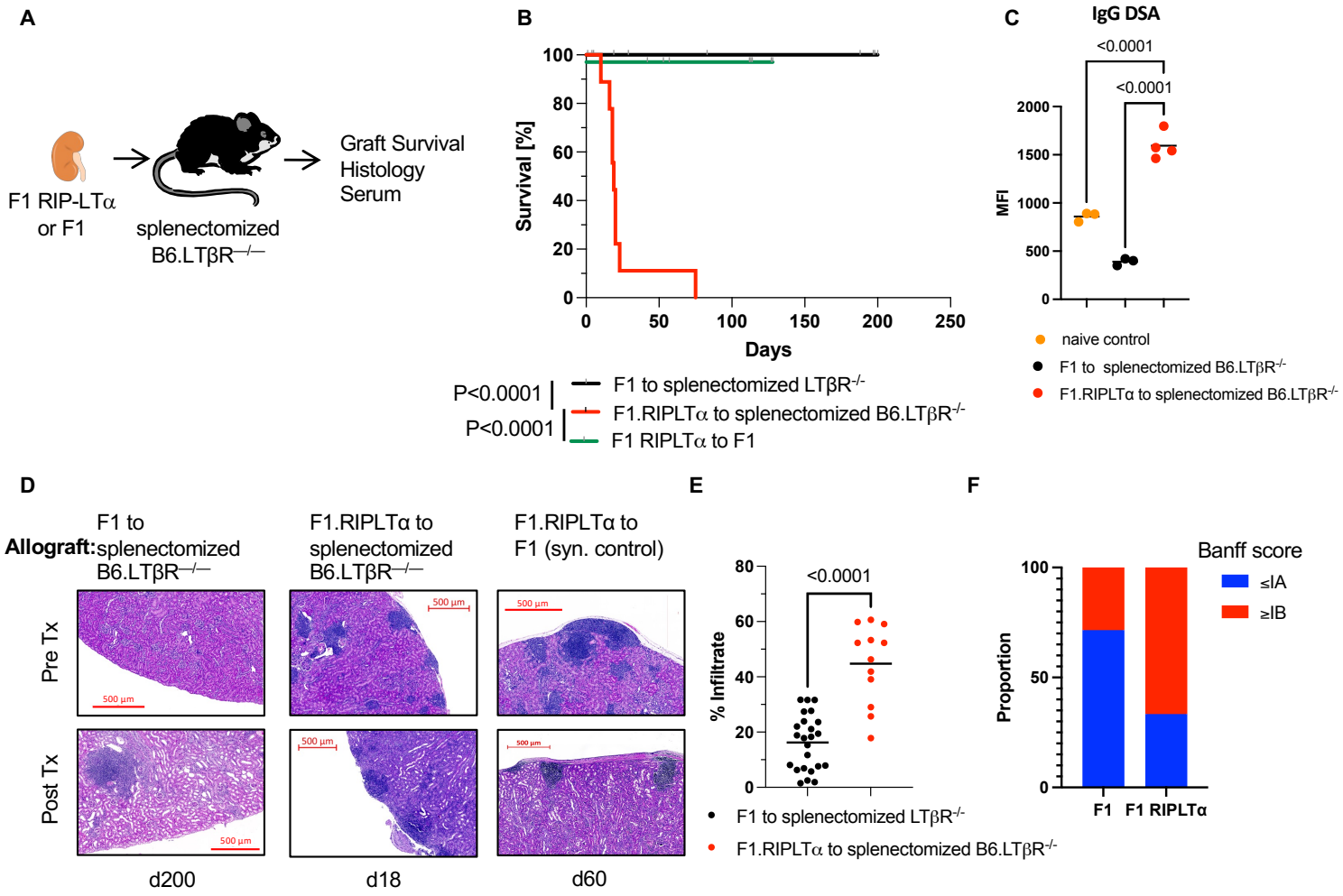
A
F1 RIP-LTα or F1
splenectomized B6.LTβR−/−
Graft Survival
Histology
Serum
B
Survival [%]
Days
P<0.0001
P<0.0001
F1 to splenectomized LTβR-/-
F1.RIPLTα to splenectomized B6.LTβR-/-
F1 RIPLTα to F1
C
IgG DSA
<0.0001
<0.0001
MFI
naive control
F1 to splenectomized B6.LTβR-/-
F1.RIPLTα to splenectomized B6.LTβR-/-
D
Allograft:
F1 to splenectomized B6.LTβR−/−
F1.RIPLTα to splenectomized B6.LTβR−/−
F1.RIPLTα to F1 (syn. control)
Pre Tx
Post Tx
500 µm
d200
d18
d60
E
<0.0001
% Infiltrate
F1 to splenectomized LTβR-/-
F1.RIPLTα to splenectomized B6.LTβR-/-
F
Banff score
≤IA
≥IB
Proportion
F1
F1 RIPLTα

Figure 1

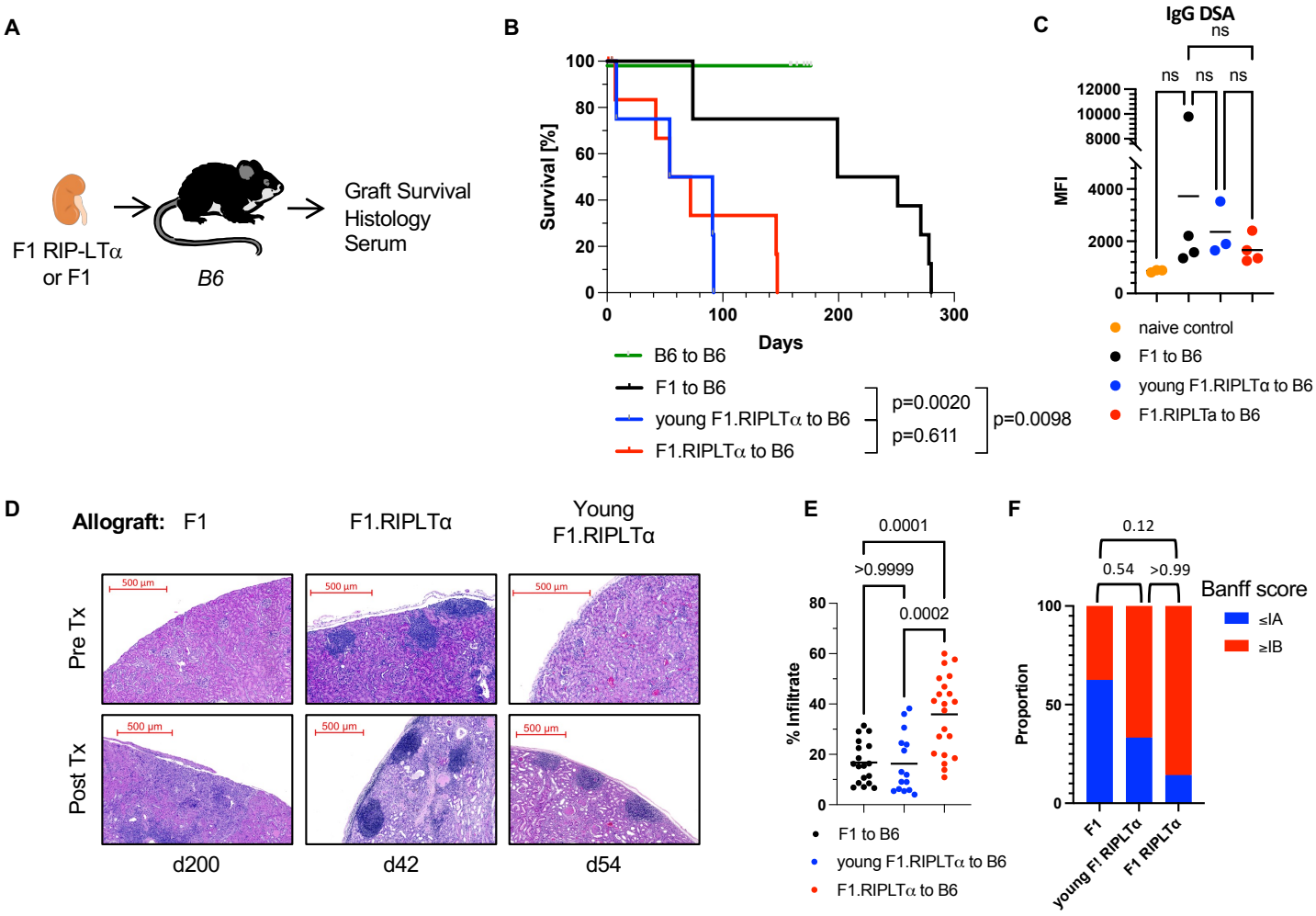
A
F1 RIP-LTα
or F1
B6
Graft Survival
Histology
Serum
B
Survival [%]
Days
B6 to B6
F1 to B6
young F1.RIPLTα to B6
F1.RIPLTα to B6
p=0.0020
p=0.611
p=0.0098
C
IgG DSA
ns
MFI
naive control
F1 to B6
young F1.RIPLTα to B6
F1.RIPLTa to B6
D
Allograft: F1
F1.RIPLTα
Young F1.RIPLTα
Pre Tx
Post Tx
500 µm
d200
d42
d54
E
% Infiltrate
0.0001
>0.9999
0.0002
F1 to B6
young F1.RIPLTα to B6
F1.RIPLTα to B6
F
Proportion
0.12
0.54
>0.99
Banff score
≤IA
≥IB
F1
young F1 RIPLTα
F1 RIPLTα

Figure 2

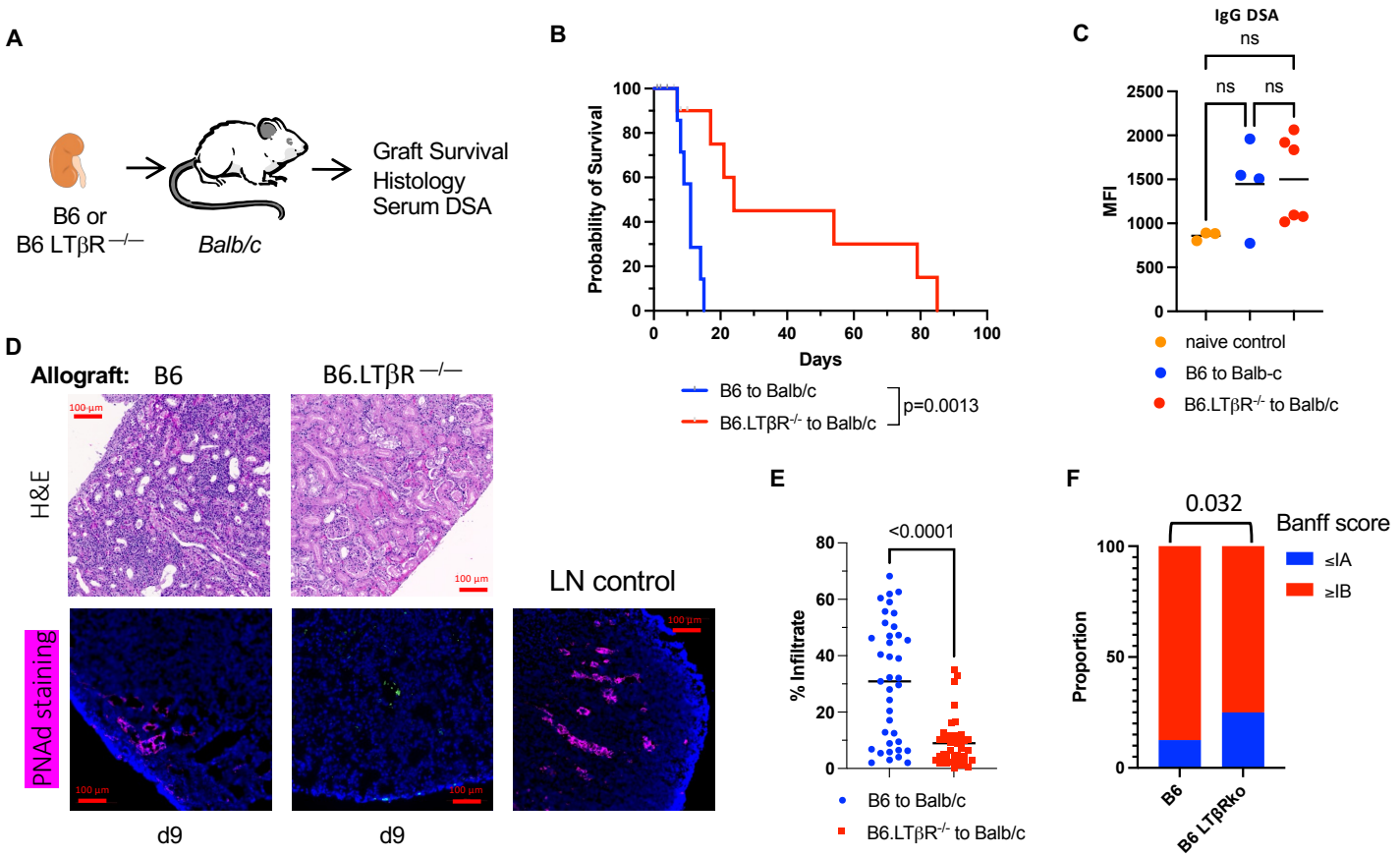
A
B6 or
B6 LTβR−/−
Balb/c
Graft Survival
Histology
Serum DSA
B
Probability of Survival
Days
B6 to Balb/c
B6.LTβR-/- to Balb/c
p=0.0013
C
IgG DSA
ns
ns
ns
MFI
naive control
B6 to Balb-c
B6.LTβR-/- to Balb/c
D
Allograft: B6
B6.LTβR −/−
H&E
PNAd staining
LN control
d9
d9
E
<0.0001
% Infiltrate
B6 to Balb/c
B6.LTβR-/- to Balb/c
F
0.032
Banff score
≤IA
≥IB
Proportion
B6
B6 LTβRko

Figure 3

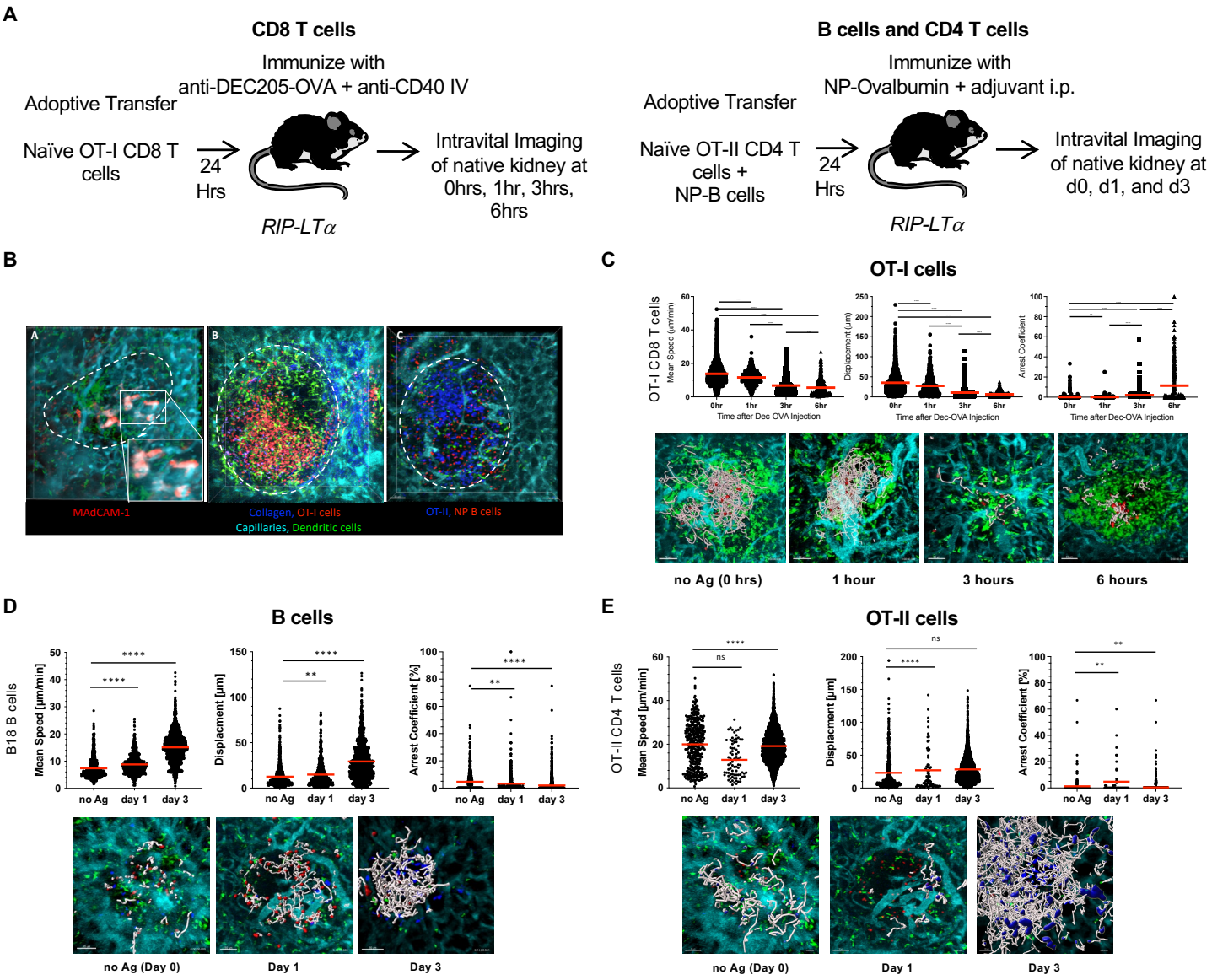
A
CD8 T cells
Immunize with
anti-DEC205-OVA + anti-CD40 IV
Adoptive Transfer
Naïve OT-I CD8 T cells
24 Hrs
RIP-LTα
Intravital Imaging of native kidney at 0hrs, 1hr, 3hrs, 6hrs
B cells and CD4 T cells
Immunize with
NP-Ovalbumin + adjuvant i.p.
Adoptive Transfer
Naïve OT-II CD4 T cells + NP-B cells
24 Hrs
RIP-LTα
Intravital Imaging of native kidney at d0, d1, and d3
B
MAdCAM-1
Collagen, OT-I cells
Capillaries, Dendritic cells
OT-II, NP B cells
C
OT-I cells
OT-I CD8 T cells
Mean Speed (μm/min)
Displacement (μm)
Arrest Coefficient
Time after Dec-OVA Injection
no Ag (0 hrs)
1 hour
3 hours
6 hours
D
B cells
B18 B cells
Mean Speed [μm/min]
Displacment [μm]
Arrest Coefficient [%]
no Ag
day 1
day 3
no Ag (Day 0)
Day 1
Day 3
E
OT-II cells
OT-II CD4 T cells
Mean Speed [μm/min]
Displacment [μm]
Arrest Coefficient [%]
no Ag
day 1
day 3
no Ag (Day 0)
Day 1
Day 3

Figure 4